

Design of Cationic Multiwalled Carbon Nanotubes as Efficient siRNA Vectors for Lung Cancer Xenograft Eradication

Chang Guo,[†] Wafa T. Al-Jamal,[†] Francesca M. Toma,[‡] Alberto Bianco,[§] Maurizio Prato,[‡] Khuloud T. Al-Jamal,^{*,†,#} and Kostas Kostarelos^{*,†}

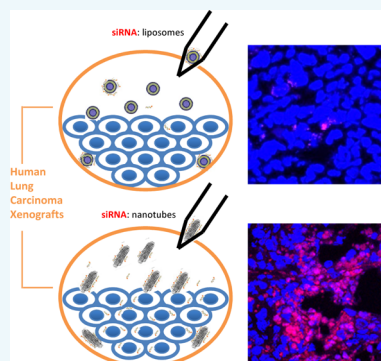
[†]Nanomedicine Lab, UCL School of Pharmacy, Faculty of Life Sciences, University College London, London WC1N 1AX, United Kingdom

[‡]Center of Excellence for Nanostructured Materials, Department of Chemical and Pharmaceutical Sciences, University of Trieste, 34127 Trieste, Italy

[§]CNRS, Institut de Biologie Moléculaire et Cellulaire, UPR 3572, Immunopathologie et Chimie Thérapeutique, 67000 Strasbourg, France

Supporting Information

ABSTRACT: Polo-Like Kinase (PLK1) has been identified as a potential target in cancer gene therapy via chemical or genetic inhibitory approaches. The biomedical applications of chemically functionalized carbon nanotubes (*f*-CNTs) in cancer therapy have been studied due to their ability to efficiently deliver siRNA intracellularly. In this study, we established the capacity of cationic MWNT-NH₃⁺ to deliver the apoptotic siRNA against PLK1 (siPLK1) in Calu6 tumor xenografts by direct intratumoral injections. A direct comparison with cationic liposomes was made. This study validates the PLK1 gene as a potential target in cancer gene therapy including lung cancer, as demonstrated by the therapeutic efficacy of siPLK1:MWNT-NH₃⁺ complexes and their ability to significantly improve animal survival. Biological analysis of the siPLK1:MWNT-NH₃⁺ treated tumors by qRT-PCR and Western blot, in addition to TUNEL staining confirmed the biological functionality of the siRNA intratumorally, suggesting that tumor eradication was due to PLK1 knockdown. Furthermore, by using a fluorescently labeled, noncoding siRNA sequence complexed with MWNT-NH₃⁺, we established for the first time that the improved therapeutic efficacy observed in *f*-CNT-based siRNA delivery is directly proportional to the enhanced siRNA retention in the solid tumor and subsequent uptake by tumor cells after local administration in vivo.



INTRODUCTION

Over the past decade, there has been exponential growth in research combining nanotechnology tools and cancer therapy. One of nanomaterials is carbon nanotubes (CNTs) which based on their structure are classified into two categories, single-walled carbon nanotubes (SWNTs) and multiwalled carbon nanotubes (MWNTs) made of single or several graphene layers rolled up into cylindrical structures, respectively. The capability of surface modification of CNTs offers an improved aqueous dispersibility hence broadening their biomedical applications, including their use as a delivery vector for various molecules in cancer therapy. Functionalized CNTs (*f*-CNTs) have been explored in almost every single modality used in cancer therapy including photothermal therapy, chemotherapy, and gene therapy.¹

In comparison to traditional chemotherapy or radiotherapy, gene therapy offers higher specificity to regulate diseases of disordered gene origin, including cancer. The induction of apoptosis has demonstrated great benefits for cancer therapy.^{2,3} One of the cancer-related genes, polo-like kinase 1 (PLK1), has been attracting increased attention in terms of cancer therapy. These highly conserved serine/threonine kinases are the

principal kinase proteins which serve as regulatory enzymes for mitotic events by performing phosphorylation at nuclear protein B23.^{4,5} They play an important role in G2-M transition and show an overexpression in a variety of tumors analyzed to date.^{6,7} Therefore, inhibition of PLK1 is predicted to block the reproduction of cancer cells, thus indicating its potential as a promising cancer drug target. Studies carried out so far have explored both chemical and genetic inhibition approaches. A chemical approach using a stilbazole compound, HMN-176, and its orally bioavailable prodrug HMN-214, have both shown potent cytotoxic activity against several tumor cell lines.⁸ Garland and co-workers believe that these compounds interact with PLK1 by interference with its normal subcellular spatial distribution at centrosomes and along the cytoskeletal structure, but not via direct inhibition. An alternative genetic approach whereby silencing PLK1 by siRNA induces apoptosis

Special Issue: Biofunctional Biomaterials: The Third Generation of Medical Devices

Received: May 1, 2015

Revised: June 1, 2015

Published: June 3, 2015

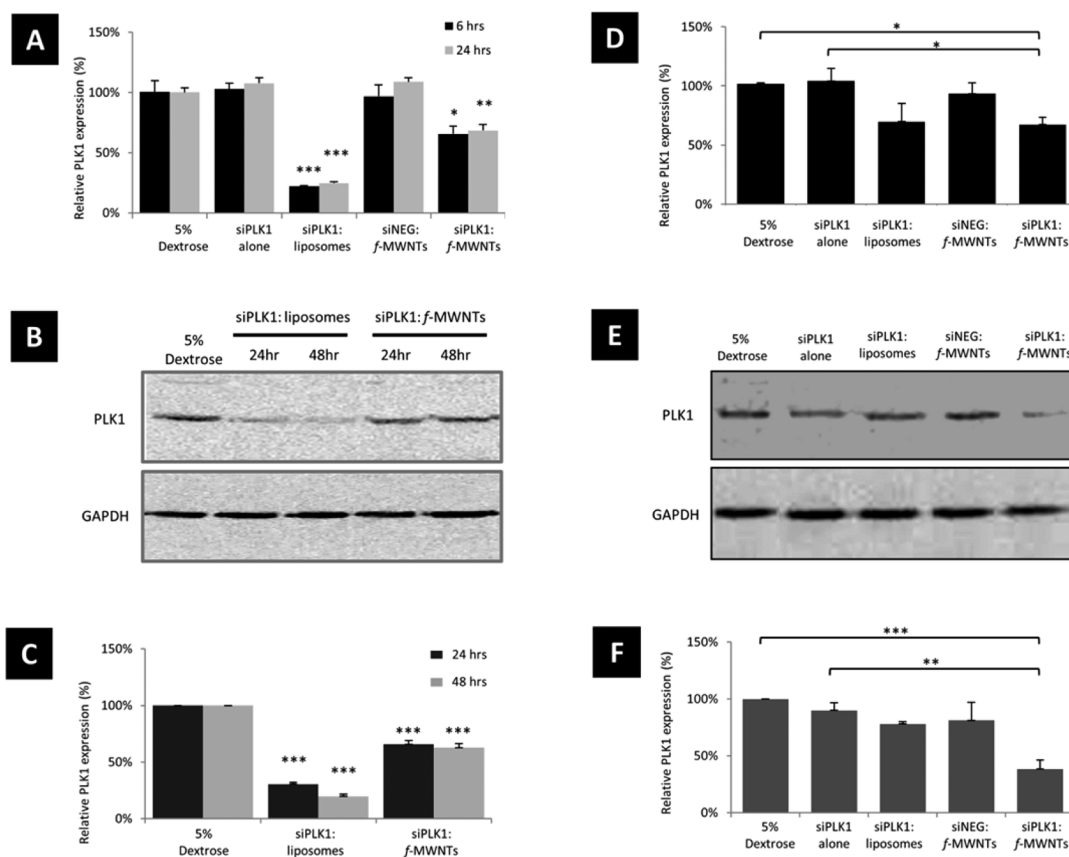


Figure 1. PLK1 gene silencing analysis in Calu6 cell lines and tumor xenografts. (A–C) In vitro gene silencing. Calu6 monolayers were treated with siPLK1 at 100 nM final concentration in serum free media for 4 h followed by incubation in complete media for another 6, 24, or 48 h. GAPDH gene was used as a control housekeeping gene. Treatment groups include 5% dextrose, siPLK1 alone, lipoplexes (siPLK1 in complex with DOTAP:cholesterol liposomes, (4:1 N/P)), siNEG:f-MWNT complexes (1:8 mass ratio), and siPLK1:f-MWNT complexes (1:8 mass ratio). (A) mRNA expression levels of PLK1 analyzed in Calu6 monolayers lysates by real time PCR ($n = 3$) at 6 or 24 h post-incubation. (B,C) Western blots of cell lysates to determine PLK1 expression at 24 or 48 h post-incubation. Both protein and mRNA levels of PLK1 were reduced more efficiently in the case of lipoplexes compared to siPLK1:f-MWNT complexes. Results were analyzed using Student's t test between treated groups and control groups (5% dextrose) at different time points, respectively. (D–F) In vivo gene silencing. Calu6 xenograft tumors were administered with siPLK1 at a dose of 4 μ g per tumor in 5% dextrose on days 17, 20, 23, 27, and 30. GAPDH gene was used as a control housekeeping gene. Treatment groups include 5% dextrose, siPLK1 alone, lipoplexes, siNEG:f-MWNT complexes, and siPLK1:f-MWNT complexes. (D) mRNA expression levels of PLK1 analyzed in Calu6 tumor lysates by real time PCR ($n = 3$) post-administration. (E,F) Western blots of cell lysates to determine PLK1 expression in the lysates. Both protein and mRNA levels of PLK1 were reduced more efficiently in the case of siPLK1:f-MWNT complexes compared to lipoplexes. Results were analyzed using Student's t test between groups of siPLK1:f-MWNT complexes and other groups (p values = * <0.05; ** <0.01; *** <0.001).

via inactivation of cyclin-dependent mitotic arrest has already shown some promising results.^{9,10} Strebhardt's group has revealed an elevated number of apoptotic nuclei, an increased sub-2N DNA content, and up to 5-fold increases in G2-M compared with controls, followed by apoptosis after depletion of PLK1 in cancer cells.^{11,12} Subsequent studies combining PLK1 gene silencing with chemotherapeutics such as paclitaxel, carboplatin, or Herceptin showed improved sensitivity of breast cancer cells against drug therapy both in vitro and in vivo.^{13,14}

f-CNTs have been employed as nonviral gene delivery vectors offering several advantages compared to alternative nonviral vectors including liposomes, cationic polymers, and cell-penetrating peptides. Advantages include efficient membrane translocation and in vivo stability.^{15,16} f-CNTs are able to deliver nucleic acids such as plasmid DNA, siRNA, or aptamers intracellularly. In these studies, siRNA:f-CNT complexation was achieved by (i) chemical conjugation of siRNA to the vector via cleavable disulfide linkage, (ii) adsorption of siRNA on the PEG-phospholipid coat adsorbed onto the SWNTs, or

(iii) by noncovalent complexation between the negatively charged siRNA and the cationic f-CNTs. Effective gene silencing was observed in all of these studies, thereby indicating the potential of CNT-based delivery of siRNA in mammalian cells. Furthermore, both SWNTs^{17–21} and MWNTs^{22–24} have shown promise as siRNA transporters in vitro and in vivo in the field of cancer therapy. In a study performed by Wang et al., f-CNT-based transfection of cyclinA siRNA was found to successfully suppress cyclinA expression, resulting in cell growth inhibition and apoptosis induction.¹⁹ Moreover, several reports have shown the therapeutic effect and suppression of tumor growth when f-CNTs were employed as siRNA delivery systems in vivo.^{18,22,25} Bartholomeusz et al. observed biological effects after exposing a wide variety of cancer cell types in vitro to siRNA:SWNT complexes. The same study showed that intratumoral administration of HIF-1 α siRNA:SWNT complexes resulted in inhibition of HIF-1 α activity in a xenograft mouse tumor model.²⁵ Furthermore, another study demonstrated that, when positively charged SWNT-CO(CH₂)₆NH₃⁺

are employed for siRNA delivery, suppression of telomerase reverse transcriptase (TERT) expression is observed both in vitro and in vivo, resulting in inhibition of the tumor growth in both murine and human tumor models.¹⁸ We have also reported antitumor activity in the human lung carcinoma (Calu6) xenograft model and prolonged animal survival by delivering a proprietary toxic siRNA sequence (siTOX using amino-functionalized multiwalled carbon nanotubes (MWNT-NH₃⁺),²² which has been also utilized in this study.

Herein, we validated PLK1 as a target in cancer gene therapy and demonstrated by combining PLK1 siRNA (siPLK1, a siRNA sequence specific for PLK1) with nanotechnology tools (*f*-CNT delivery vectors) an improved therapeutic efficacy and observed prolonged animal survival. Moreover, we explored for the first time the correlation between siRNA retention within the solid tumor together with their cellular uptake in tumor cells in vivo and the resultant therapeutic outcome. Improved tumor retention and enhanced cellular uptake of siRNA:MWNT-NH₃⁺ complexes appear to play an essential role in improving the therapeutic outcome after local administration of siRNA in vivo.

RESULTS

siPLK1 Expression in siPLK1:*f*-MWNT Complexes Treated Group. The chemical structure of *f*-MWNT (MWNT-NH₃⁺) studied here is shown in Figure S1. To validate the PLK1 siRNA (siPLK1) sequence in vitro, Calu6 cells were incubated with siPLK1:*f*-MWNT complexes (1:8 mass ratio) for 24 or 48 h. The level of PLK1 expression in Calu6 cells was assessed by real-time PCR and Western blotting (Figure 1A,B,C). GAPDH was used as a housekeeping gene for real-time PCR and as a control for Western blotting. Lipoplexes formed by complexation of siPLK1 and cationic liposomes (DOTAP:cholesterol) were included in the study as a benchmark transfecting reagent. There was a clear difference in gene silencing efficacy between the two vectors in vitro, where lipoplexes exhibited more efficient PLK1 gene knock-down than siPLK1:*f*-MWNT complexes as measured by PLK1 protein level (Figure 1A,B). Protein expression was reduced to 30% ± 1% and 20% ± 2% after 24 and 48 h, respectively, in the case of the lipoplex transfection, compared to only 66% ± 3% and 63% ± 4% in the case of transfection using siPLK1:*f*-MWNT complexes after the same incubation times (Figure 1B). Figure 1C shows that incubation of Calu6 cells with siRNA:*f*-MWNT complexes decreased the number of mRNA copies of the PLK1 to 66% ± 9% and 68% ± 4% at 6 and 24 h, respectively, as shown by real-time PCR. In comparison, incubation of Calu6 cells with lipoplexes attenuated relative PLK1 mRNA level to 22% ± 1% and 25% ± 1% at 6 and 24 h, respectively. Hence, we concluded that more potent gene silencing could be achieved using the lipoplexes than siRNA:*f*-MWNT complexes in vitro.

We then investigated whether siPLK1 is still active under biological conditions in vivo. siPLK1 was complexed with either *f*-MWNTs or cationic liposomes and directly introduced into Calu6 tumors by intratumoral injection. PLK1 mRNA transcripts and protein were extracted from injected tumors and PLK1 expression was evaluated by real-time PCR and Western blotting (Figure 1D,E,F) in all groups. Negative siRNA siNEG:*f*-MWNTs treated group was included to eliminate any nonspecific toxicity of the siRNA or the *f*-MWNTs. Both techniques demonstrated a significant reduction in PLK1 mRNA transcripts and protein levels in the tumors

treated with siPLK1:*f*-MWNT complexes compared to the injected tumors of control groups (5% dextrose dextrose and siPLK1 alone) tumors. Intratumoral injection of siPLK1:*f*-MWNT complexes reduced PLK1 mRNA levels to 67% ± 6% and PLK1 protein levels to 38% ± 8% relative to expression of the housekeeping gene GAPDH (Figure 1D,E,F). Lipoplexes and siNEG:*f*-MWNT treated groups exhibited different effects in PLK1 silencing both in vitro and in vivo. Such results proposed that siPLK1:*f*-MWNT complexes as promising vectors for RNAi in vivo. Furthermore, the delivery capacity of well-established delivery vectors such as liposomes which have been shown to be potent in vitro can be compromised when administered locally within tumor environment in vivo.

Tumor Growth and Animal Survival in Vivo after Intratumoral Administration of siPLK1:*f*-MWNT Complexes. We further studied whether gene silencing by siPLK1:*f*-MWNT complexes is sufficient to delay tumor growth and improve animal survival. For this purpose, treatments were injected intratumorally in an established human lung Calu6 xenograft tumor model. Tumor growth was monitored by measuring the tumor size three times per week with Vernier calipers over a period of 30 days. Figure 2A showed a significant inhibition in tumor growth observed in siPLK1:*f*-MWNT complex-treated group. Reductions in tumor volume were noticeable after the second therapeutic injection. Other treatment groups (siPLK1 alone, siPLK1:liposomes, siNEG:*f*-MWNT complexes) showed no difference in volume compared to the 5% dextrose treated group. To compare the efficiency of different types of therapies used, quadrupling time was calculated and expressed in Figure 2B. Quadrupling time of siPLK1:*f*-MWNTs treated group was 20.5 ± 2.3 days (*n* = 9) compared to only 11.3 ± 0.4 days (*n* = 10) in the case of the 5% dextrose treated group. The siPLK1:*f*-MWNT group exhibited a significant increase in quadrupling time compared to all other treated groups. Animal survival analysis is shown in Figure 2C. The siPLK1:*f*-MWNT complex-treated group showed a significant increase in animal survival compared to all other groups (5% dextrose, siPLK1 alone, siPLK1:liposomes, siNEG:*f*-MWNT complexes). There was no significant improvement in animal survival for those treated with siPLK1:liposomes compared to 5% dextrose or siPLK1 alone.

Observation of siPLK1:*f*-MWNT Complexes in Tumor Mass and the Toxicity of *f*-MWNT Vehicle to Tumor Cells. Tumors were excised when the tumors reached their maximum growth volume allowed by the UK Home Office. Figure 3 shows a representative cross section image of the whole tumor from each treatment group. The presence of *f*-MWNT in siNEG:*f*-MWNT and siPLK1:*f*-MWNT-treated tumors was confirmed by the grayish color in the core of these tumors (at 100× magnification). Tumors were fixed in formalin and processed for either neutral red or H&E staining in order to perform histological examination of the tumors at the microscopic level. Neutral red staining (at 400× magnification) confirmed the presence of *f*-MWNTs in tumor cells. Moreover, H&E staining revealed extended necrosis in the areas around the CNTs only in the siPLK1:*f*-MWNT treated group. Tumors treated with siNEG:*f*-MWNT complexes lacked areas of necrotic tissues that were apparent in the siPLK1:*f*-MWNTs group, indicating that the toxicity seen was due to siPLK1 silencing after being internalized into the cells. Major organs such as heart, spleen, lung, liver, and kidney were also dissected and sectioned for neutral red and H&E staining (SI Figure S2). However, *f*-MWNTs could not be detected in these organs,

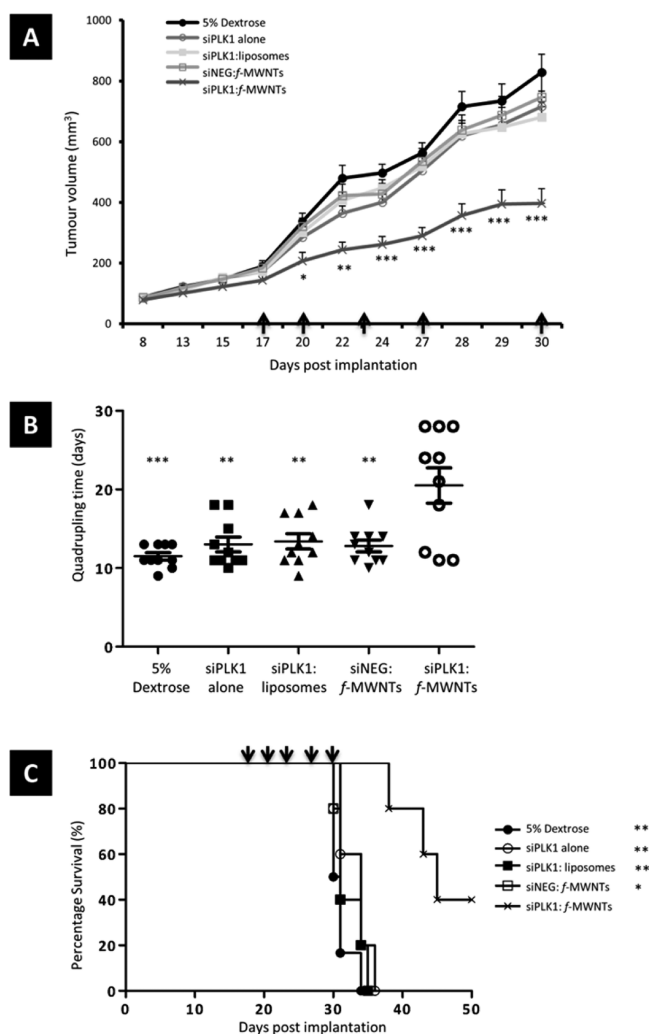


Figure 2. Tumor growth and survival curves in Calu6 xenograft-bearing mice. (A) Growth curve analysis of Calu6 xenografts. Female Swiss nude mice Calu6 xenograft tumors were administered with siPLK1. Treatment groups include siPLK1 (4 μ g) in complex with either *f*-MWNTs (1:8 mass ratio) or DOTAP:cholesterol liposomes (N/P = 1/4; 4 μ g siRNA). siNEG:*f*-MWNT (1:8 mass ratio) complexes and siPLK1 alone were injected as negative controls. Arrowheads indicate injections on days 17, 20, 23, 27, and 30. Results were presented as mean \pm SEM ($n = 9-10$). (B) Tumor volume quadrupling times (TVQT, in days) for treatment and control groups. (C) Survival analysis of Calu6 xenograft bearing mice. Formulations: 5% dextrose as control (circle); siPLK1 alone (4 μ g) (open circle); lipoplexes (N/P = 1/4; 4 μ g siRNA) (square); siNEG:*f*-MWNT complexes (mass ratio = 1:8; 4 μ g siRNA) (open square); siPLK1:*f*-MWNT complexes (mass ratio = 1:8; 4 μ g siRNA) (star). Results were analyzed using Student's *t* test between groups of siPLK1:*f*-MWNT complexes and other groups (p values = * <0.05; ** <0.01; *** <0.001).

indicating there was retention of the vectors in tumor tissue after intratumoral injection.

Apoptosis Induction in Tumor Mass by PLK1 Silencing. To confirm whether apoptosis was the mechanism of cell death as a result of PLK1 silencing, TUNEL staining was performed and all nuclei were counterstained by using DAPI stain (Figure 4). Only apoptotic cells exhibited green fluorescence (TUNEL positive). siPLK1:*f*-MWNT treated tumors were TUNEL positive in the same regions where *f*-MWNTs were abundant as confirmed by DIC images. Similar

tumor regions exposed to siNEG:*f*-MWNT complexes were TUNEL negative. This result further confirms that apoptosis may be attributable to cell death induced by PLK1 gene silencing. The groups treated with 5% dextrose and lipoplexes showed a predominantly healthy appearance with scarce areas of TUNEL positive cells which could be due to a natural process of cell death during tumor growth.

siRNA Retention in Tumor Mass after Local Administration of siRNA: *f*-MWNT Complexes. In order to investigate the kinetics of siRNA clearance from the tumor mass and more importantly to learn about the interaction between siRNA and tumor cells, we have substituted the siPLK1 with fluorescently labeled negative siRNA with AlexaFluor AF546 (siNEG AF546). Whole body imaging in addition to imaging of excised tumors (*ex vivo*) was carried out after single intratumoral injections (SI Figure S3 and Figure 5) using the Xenogen IVIS imaging system to visualize the fluorescence signal representing siNEG AF546 complexed with both *f*-MWNT and liposomes. It was clear from whole body imaging that the lipoplex group exhibited long-lasting retention in the tumor mass up to 24 h (47.5% ID \pm 3.0% ID after 1 h and 21.3% ID \pm 4.6% ID after 4 h, $n = 6$). On the contrary, siNEG AF546 alone cleared rapidly from the tumor mass with 26.6% ID \pm 3.8% ID ($n = 6$) and 8.9% ID \pm 2.0% ID detected in the tumors after 1 and 4 h, respectively (SI Figure S3). Interestingly, the siNEG AF546:*f*-MWNT treated group exhibited lower signals compared to the lipoplex formulation by whole body imaging technique, with 62.3% ID \pm 6.3% ID and 15.2% ID \pm 1.5% ID ($n = 6$) remaining within the tumor mass at 1 and 4 h postinjection, respectively.

Imaging of tumors (*ex vivo*) was then performed to account for problems associated with deep tissue penetration of fluorescence signals (Figure 5). Tumors were dissected 24 h after intratumoral administration of free or complexed siNEG AF546 and observed under Xenogen IVIS imaging system (Figure 5A). Similar tumor retention profiles were obtained *ex vivo* as those obtained by whole body imaging. To confirm whether the fluorescence detected by IVIS was associated with tumor cells or within the interstitial space, tumor masses were excised, cryo-sectioned, postfixed, and examined by confocal laser scanning microscopy (CLSM) (Figure 5B). During the fixation and subsequent washing steps, free nonassociated siNEG AF546 was thus eliminated before imaging by CLSM. At 24 h post-intratumoral administration, the siNEG AF546 treated group showed no fluorescence signals indicating that siRNA alone was not able to internalize into cancer cells without the aid of a delivery system. siNEG AF546:*f*-MWNT complex treated tumors showed intense red fluorescence signals confirming intracellular delivery of siNEG AF546 by means of *f*-MWNTs. Moreover, fluorescence signals in the latter group were extended throughout the cells including the nucleus. Such results were compatible with the results we previously obtained in cancerous cell monolayer studies.^{26,27} Surprisingly and contrary to whole tumor imaging studies (Figure 5A), intracellular delivery of siNEG AF546 by lipoplexes appeared to be less intense than the *f*-MWNT-mediated delivery. Such results were in line with the reduced gene silencing efficiency obtained in the case of the cationic liposome-mediated delivery compared to the nanotube-mediated delivery *in vivo*.

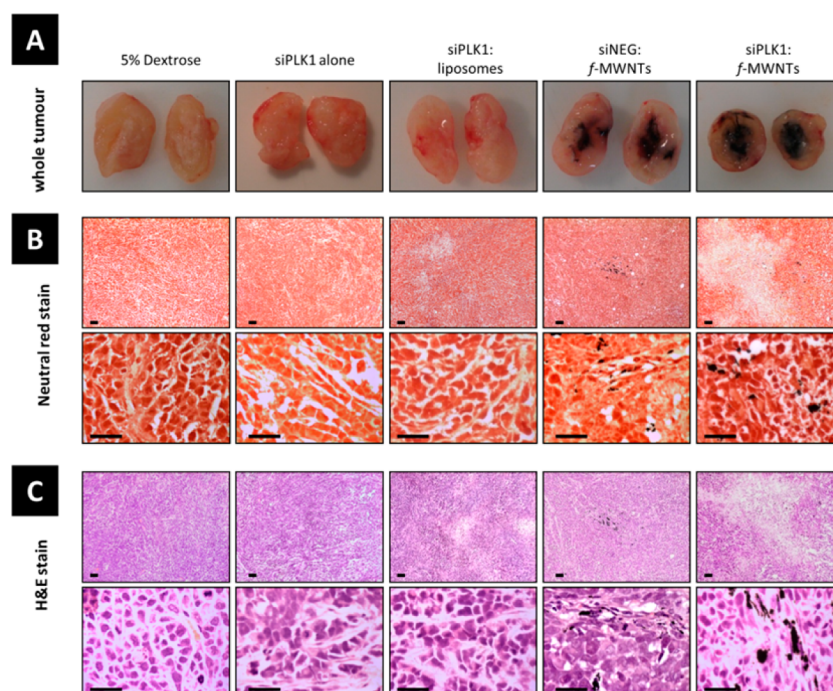


Figure 3. Histological analysis of Calu6 tumor xenografts. (A) Photographs of whole tumors excised once reaching 800 mm³ volume. Histological examination of fixed tumor sections processed for routine histology with (B) neutral red stain or (C) and hematoxylin and eosin (H&E) stain. Tumors treated with siPLK1:*f*-MWNT complexes showed significant tissue necrosis compared to all other treated groups.

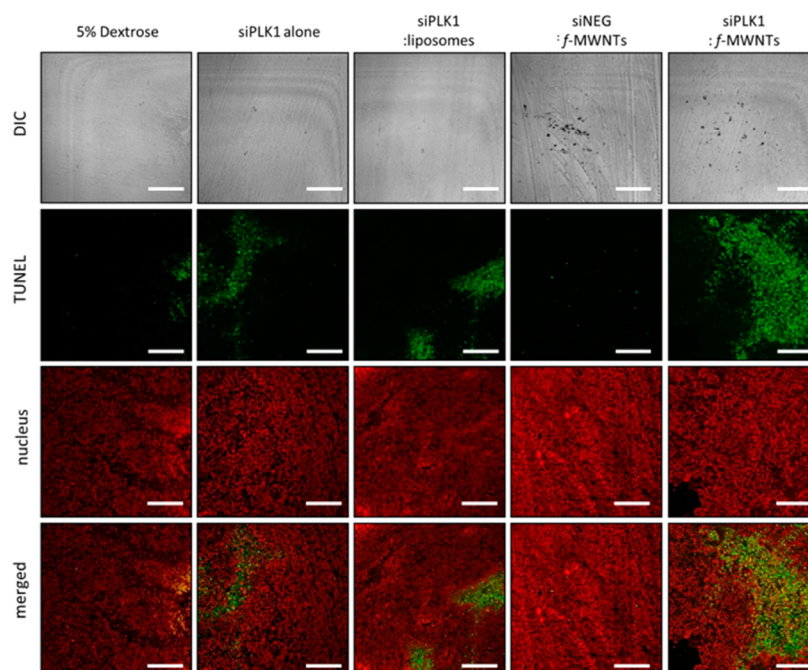


Figure 4. TUNEL analysis of Calu6 tumor xenografts. Tumor sections were deparaffinized and rehydrated through graded ethanol, then TUNEL stained to identify apoptotic (green) cells from counterstained nuclei (red). Phase contrast images of corresponding fields of view shown to indicate MWNT-NH₃⁺ localization in tumor tissues. Tumors treated with siPLK1:*f*-MWNT complexes showed significant apoptosis of the tumor cells. Scale bar is 200 μm.

DISCUSSION

We have previously reported the most comprehensive and promising study to date describing tumor apoptosis, delayed tumor growth, and prolonged survival of human lung xenograft bearing mice after intratumoral administration of siRNA:*f*-MWNT complexes.²² In this previously reported study, we

observed significant improvements in the therapeutic outcome in the group treated with siRNA:*f*-MWNT complexes compared to the lipoplex treated group. That study utilized the proprietary sequence siTOX to induce tumor apoptosis and death, while ammonium functionalized MWNT and cationic liposomes were used as delivery vectors for the siRNA molecules. Although it was essential to investigate the reason

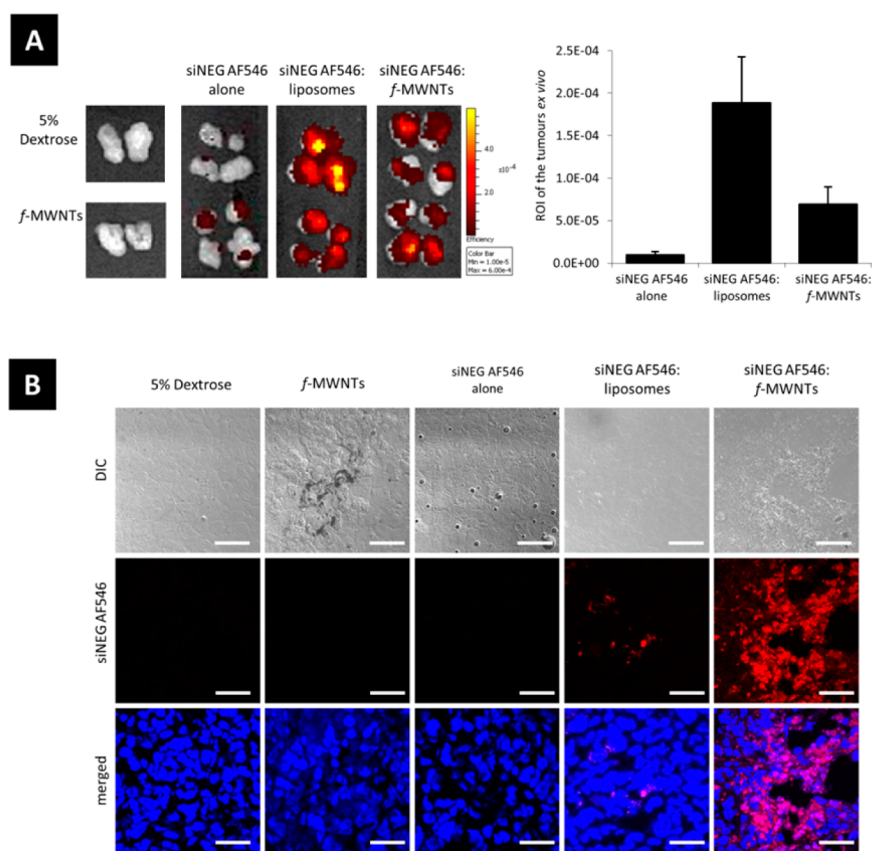


Figure 5. Uptake of siNEG AF546 in tumor xenografts. (A) Ex vivo imaging (left) and quantification of the fluorescence signals (right) detected from the dissected tumors by Xenogen IVIS imaging system. Tumors were dissected 24 h after intratumoral administration of siNEG AF546 in free or complexed forms. (B) Intracellular uptake of siNEG AF546 in the dissected tumors by CLSM. Scale bars, 50 μ m.

behind the drastically improved performance of the ammonium functionalized MWNTs over cationic liposome vectors for siRNA delivery in vivo, due to the unknown nature of siTOX, it was difficult to perform a direct comparison between the two delivery systems at the molecular level (e.g., mRNA and protein synthesis level). Therefore, it was deemed essential to carry out further studies to correlate the pharmacokinetic profiles with bioactivity of the siRNA delivered by means of the two fundamentally different delivery systems. In this study the siTOX was substituted with a siRNA sequence specific for PLK1, a gene known to play an important role in cancer cell replication and proliferation, so successful gene silencing could lead to tumor growth arrest. Furthermore, we performed mechanistic studies substituting functional siRNA with fluorescently labeled noncoding siRNA (siNEG) in order to determine the siRNA uptake into tumor mass in vivo and its retention in the tumor following intratumoral administration.

The main finding was that complexation of siPLK1 with MWNT-NH₃⁺ facilitated its internalization by tumor cells in solid tumor mass in vivo, resulting in significant PLK1 knockdown compared to the equivalent lipoplex formulation and all other treated groups. We did not observe significant inhibition in tumor growth when treated with lipoplexes in our study although the lipoplexes worked in vitro (Figure 1A–C). This could be due to the retention of lipoplexes into the tumor after intratumoral injection was not good and they were washed quickly while the CNT complexes were retained within the tumor so were longer acting, as observed from the 24 h retention of fluorescence based siNEG AF546 in the free or complexed forms after intratumoral administration (Figure 5B).

Pharmacokinetic studies suggested that the bioavailability of siRNA within tumor cells after complexation with carbon nanotubes compared to the cationic liposomal formulation could be the rationale behind the superior bioactivity of the former delivery system. Whole tumor imaging by IVIS imaging system showed high fluorescence signals in tumors injected with the cationic liposomal formulation which was surprising and contradicting the bioactivity results. However, further inspection of tumor masses microscopically by CLSM confirmed that the majority of the siRNA was not delivered inside the cell and rather was retained in the interstitial space of the tumor in the case of the cationic liposome-based vectors. Noninternalized siRNA was most likely eliminated during the process of washing and fixation prior to imaging by CLSM, while internalized siRNA was resilient to washing and was therefore visualized inside the cells by CLSM as was the case for *f*-MWNT-based carriers.

Cationic liposome based siRNA nanocarriers have been widely used for cancer therapy in different tumor models. These complexes were usually injected systemically²⁸ that may explain the less therapy effects in our case. Previous studies have shown that liposomal systems exhibit broad interstitial diffusion within tumor mass after intratumoral injection, with slow clearance from the interstitial space.²⁹ Prolonged accumulation of liposomes and the therapeutics within tumor mass does not always lead to enhanced intracellular delivery, as it is necessary to establish if binding to the extracellular matrix does not hinder intracellular uptake into tumor cells. In conclusion of this study, carbon nanotube-mediated delivery exhibited the highest uptake in tumor cells as obtained by

CLSM, which conflicts with the results obtained by whole body IVIS imaging which showed higher fluorescence signals of tumors injected with the lipoplexes. It is evident that detailed mechanistic studies utilizing multiple techniques are necessary for expressing the delivery efficiency of various delivery systems. Results obtained in this study demonstrated a lack of toxicity of *f*-MWNTs and their efficiency as cytosolic siRNA carriers, in addition to the bioactivity of the delivered siRNA as demonstrated by efficient gene silencing *in vivo* superseding the efficiency of cationic liposomal vectors, as previously reported in other studies using stroke and cancer disease models.^{15,22}

Interestingly, amino functional groups on the MWNT-NH₃⁺ sidewalls can be further modified such as building dendritic structures as reported previously.^{26,27} Engineering the degree and type of dendritic branching is expected to affect the degree of siRNA association and gene silencing efficiency. We concluded from previous *in vitro* studies^{26,27} that increasing the degree of the dendritic branching on the *f*-MWNT side walls improved their water dispersibility, individualization, and siRNA complexation. Future work should focus on comparing the bioactivity and pharmacokinetic profiles of other types of dendritic *f*-MWNT generations for siRNA delivery *in vivo*. In conclusion, we reformulated MWNT-NH₃⁺ by complexing with siPLK1 or siNEG AF546, to elucidate and understand of the efficient siRNA delivery in xenograft tumors. We proved that cationic multiwalled carbon nanotubes are efficient siRNA vectors for tumor eradication *in vivo*.

This work is a proof-of-principle study demonstrating that biocompatible *f*-MWNTs are effective intracellular transporters for siRNA in cancer gene therapy *in vivo*. So far, only a limited number of studies have reported *f*-CNTs as siRNA delivery systems for *in vivo* applications for diseases other than cancer. Lanner et al. presented successful CNT-based transfection of TRPC3 siRNA in adult skeletal muscle cells. The TRPC3 protein expression was knocked down, with functional effects seen in the inhibition of DAG-induced Ca²⁺ and decreases in the insulin-mediated glucose uptake.³⁰ This validated TRP3 as a target for treatment of insulin-resistant conditions. Moreover, evidence has also shown that *f*-CNTs can effectively aid the transfection of cells thus helping the gene delivery, such as T cells and primary cells, including neurons and cardiomyocytes.^{31–34} Very recently, we reported MWNT-NH₃⁺ as transporters for Caspase-3 siRNA for the prevention of apoptosis following stroke induction in a murine Endothelin-1 stroke model. Functional recovery was achieved to perilesional levels after stereotactic administration of the therapy in both pre- and postlesioned animals.¹⁵ Overall, although *f*-CNT-mediated gene silencing is at an early preclinical stage, recent studies have shown that *f*-CNTs offer significant benefits in the area of gene therapy and, more specifically, gene silencing.

EXPERIMENTAL SECTION

Materials. MWNTs were purchased from Nanostructured & Amorphous Materials Inc., Houston, TX; Stock no 1240XH, 95%, OD 20–30 nm. MWNT-NH₃⁺ was prepared as previously described.²⁷ Chemicals and solvents were obtained from Sigma-Aldrich (USA) and they were used as received. Liposomes were prepared by lipid film hydration, followed by filtration. Briefly, DOTAP:cholesterol (2:1 molar ratio) was dissolved in chloroform:methanol (4:1 v/v), the organic solvent was evaporated in a rotary evaporator (Buchi, Switzerland) under vacuum at 40 °C for 30 min and then flushed with a N₂ stream

to remove any residual traces of organic solvent. The dried lipid film was hydrated with 1 mL of 5% dextrose, sonicated, and extruded twice through 0.1 μm filter under sterile conditions. The final lipid concentration was 2 mM. AlexaFluor 546-labeled siNEG (siNEG AF546) (5′ → 3′: UGCGCUACGAUCGACG-AUG) and siPLK1 (5′ → 3′: CCUUGAUGAAGAAGAUAC) were purchased from Eurogentec (UK). Advanced RPMI, fetal bovine serum (FBS), penicillin/streptomycin, and phosphate buffered saline (PBS) were from Gibco, Invitrogen (UK). Human lung carcinoma Calu6 (HTB-55) were from ATCC (UK). BCA Protein assay kit, paraformaldehyde (PFA), Restore Plus Western Blot Stripping Buffer, and ECL detection system were purchased from Thermo Scientific Ltd. (USA). Mouse monoclonal GAPDH antibody were obtained from Ambion (Austin, USA) and HRP-linked antimouse IgG was obtained from Jackson ImmunoResearch (West Grove, MA, USA). Mouse monoclonal PLK1 antibody was purchased from Abcam (Cambridge, UK) and HRP-linked anti-rabbit IgG was obtained from Cell Signaling (MA, USA). Vectashield mounting media with DAPI (H1200) was purchased from Vector Laboratories (USA). Hybond ECL nitrocellulose membranes were obtained from GE Healthcare (UK). Complete Protease Inhibitor cocktail is from Roche. Unless otherwise stated, all others reagents were obtained from Sigma.

Liposome: siRNA and siRNA:MWNT-NH₃⁺ Complexation for Biological Studies. siRNA complex preparations for *in vivo* experiments were carried out by diluting the appropriate volume of liposome (1.4 mg/mL) or MWNT-NH₃⁺ (1.28 mg/mL) dispersion to a total volume of 25 μL in 5% dextrose, to achieve siRNA; liposomes N/P = 4 or siRNA:MWNT-NH₃⁺ mass ratio = 8. siRNA initial stock was prepared at 20 μM. An equal volume of 160 μg/mL siRNA in 5% dextrose was then added to the liposome or MWNT-NH₃⁺ aliquots and mixed by rapid pipetting, yielding a final siRNA concentration of 80 μg/mL. Fifty microliters of the complexes was injected per animal. A similar procedure was used to prepare complexes for *in vitro* experiments except that complexation was carried out initially in a total volume of 100 μL, then diluted 5× with serum-free media yielding siRNA final concentration of 100 nM.

In Vitro PLK1 Gene Silencing in Calu6 Cells and In Vivo PLK1 Gene Silencing in Calu6 Xenograft Tumors. Calu6 cells (30 000 cells/well) were seeded in 6-well plates. Twenty-four hours later, cells were transfected with siPLK1 in different formulations. After 6, 24, or 48 h post-transfection, cells were washed twice with ice-cold PBS before lysis. Tumor tissues were harvested and snap-frozen immediately in liquid-nitrogen-cooled isopentane. Samples were stored at −80 °C prior to lysis. The tumors were placed in liquid nitrogen and ground thoroughly with a pestle. Decanted tissue powder was weighed in Eppendorfs before lysis.

Gene Silencing by Western Blot. Cells or decanted tissue powder were collected directly into lysis buffer (50 mM Tris-Cl, pH 8.0, 150 mM NaCl, 0.1% SDS, 1% Nonidet P-40, and 0.5% sodium deoxycholate). The tumor tissue lysate was sonicated and then left on ice for 30 min. Samples were cleared by centrifugation at 15 000 rpm for 15 min at 4 °C and the supernatant was collected. Total protein concentration was assessed using BCA Protein assay kit, and 10 μg of total protein was taken from each supernatant and resolved on 10% SDS-PAGE gels and transferred to Hybond ECL nitrocellulose membranes. After blocking in 3% BSA for overnight, the blots were incubated with rabbit monoclonal PLK1 antibody at

1:1000 dilution, followed by horseradish peroxidase (HRP)-linked anti-mouse IgG at 1:10 000 dilution used as secondary antibody. The specific bands were detected with enhanced chemiluminescence (ECL) detection system. Band intensities of the PLK1 were quantified by *ImageJ*. GAPDH was used as an internal reference (housekeeping) gene. Membranes were stripped, blocked, and rehybridized with mouse anti-GAPDH antibody (1:4000 dilution), followed by incubation with HRP-conjugated antibody.

Gene Silencing by Real-Time PCR Analysis. Total RNA was extracted with an RNeasy Mini Kit (QIAGEN) according to the manufacturer's instructions. The concentration of total RNA was determined by measuring the optical density at 260 nm and the purity was checked as the 260 nm/280 nm ratio with expected values between 1.8 and 2.0. The first strand of cDNA was prepared from 1 μ g RNA in a total volume of 20 μ L using the QuantiTect Reverse Transcription Kit (QIAGEN). Real-time PCR was performed using the CFX96 Real-Time PCR Detection System (BioRad). The reactions contained 1 \times Fast SYBR Green Master Mix (BioRad), each primer (h-PLK1 sense 5' ACA GTA TTC CCA AGC ACA TC3'; h-PLK1 antisense 5' AAT GGT CAG GCA GGT GAT 3'; h-GAPDH sense 5' GGT CGG AGT CAA CGG ATT 3'; h-GAPDH antisense 5' ATC GCC CCA CTT GAT TTTG 3') at 200 nM and 1 μ L of cDNA from reverse transcription PCR in a 25 μ L reaction. After an initial denaturation step at 95 $^{\circ}$ C for 10 min, amplification was carried out with 40 cycles of denaturation at 95 $^{\circ}$ C for 10 s and annealing at 60 $^{\circ}$ C for 30 s. Amplification was followed by a melting curve analysis to confirm PCR product specificity. No signals were detected in no-template controls. All samples were run in triplicate and the mean value of each triplicate was used for further calculations. Relative gene expressions were calculated using the $\Delta\Delta C_T$ method. The quantity of GAPDH (housekeeping) transcript in each sample was used to normalize the amount of PLK1 transcripts, and then the normalized value was compared to the normalized expression in naive cells to calculate a fold change value.

Tumor Xenograft Animal Model and Survival Studies.

All animal experiments were performed in compliance with the UK Home Office Code of Practice for the Housing and Care of Animals Used in Scientific Procedures. Six- to eight-week-old female Swiss nude mice (Charles River Laboratories, UK) were caged in individually vented cages (IVC; Allentown, USA) in groups of four with free access to food and water. A temperature of 19–22 $^{\circ}$ C was maintained, with a relative humidity of 45–65%, and a 12 h light/dark cycle. An established human lung Calu6 xenograft tumor model was applied as described previously.²² Mice were inoculated subcutaneously with 1×10^6 Calu6 human epithelial lung carcinoma cells mixed 1:1 with Matrigel (Becton Dickinson, UK) in 100 μ L on the both flanks subcutaneously. Intratumoral injections were performed when the tumor volume reached 0.2–0.4 cm^3 and were carried out on days 17, 20, 23, 27, and 30 post-tumor implantation in this study. For intratumoral administration and tissue analysis, mice were anesthetized using isoflurane and injected with the siRNA alone or the complexed prepared in 5% dextrose. The needle was inserted in the longitudinal direction from the tumor edge into the center of the tumor, 50 μ L of the dispersion was administered slowly over 1 min, and the needle was left in the tumor for another 5 min to prevent sample leakage.

Tumor growth was monitored by measuring the tumor size three times per week with Vernier calipers over a period of 30

days. The tumor volume was estimated by bilateral Vernier caliper measurement three per week and calculated using the formula (width \times width) \times (length) \times ($\pi/6$), where length was taken to be the longest diameter across the tumor. Implantation with 5% dextrose (naive), carbon nanotubes alone, and siRNA in different formulations were carried out twice weekly for all groups. Quadrupling time is used to compare the efficiency of different types of therapies used and is defined as the time required for a tumor to reach four times its initial volume at the start of the therapy.^{35,36} Mice were sacrificed by cervical dislocation when tumor area reached 800–1000 mm^3 .

Neutral Red and Hematoxylin/Eosin (H&E) Tissue Histology. For histological analysis, tumors samples and the major organs (heart, lung, liver, spleen, and kidneys) were fixed in 10% buffered formalin and processed for routine histology with neutral red and hematoxylin and eosin (H&E) stain by the Laboratory Diagnostic Service of the Royal Veterinary College (London, UK). Microscopic observation of tissues was carried out with Nikon Microphot-FXA microscope coupled with Infinity 2 digital camera.

TUNEL labeling. Tissue sections were deparaffinized in HistoClear and rehydrated through graded ethanol. The DeadEnd Fluorometric TUNEL System (Promega, UK) was used to label nicked DNA through incorporation of fluorescein-12-dUTP. Samples were incubated with recombinant Terminal Deoxynucleotidyl Transferase (rTdT) as per manufacturer's instructions and fluorescein labeling was visualized. Slices were visualized under 10 \times lens using CLSM. DAPI was used to counterstain nuclei. DAPI and fluorescein were excited at 4% of 365 and 2% of 488 laser power, respectively.

In Vivo and Ex Vivo Optical Imaging Study. Optical imaging studies were performed using an IVIS spectrum small-animal in vivo imaging system (Caliper Lifescience, Hopkinton, MA). Mice bearing Calu6 tumors were intratumorally/intratumoral injected when the tumors reached 500 mm^3 , and imaged at 5 min, 30 min, 1 h, 2 h, 3 h, 4 h, and 24 h post-administration. Isoflurane (2%) was used for anesthesia during imaging. The fluorescence images were obtained with the following settings: exposure time (1 s), f/stop (2 s), binning (4 s), and field of view (24 s). Excitation filters were 535 nm. All images were background subtracted using *Living Image* software. Tumors and different organs were dissected 24 h postinjection. Tumors were cross-sectioned with the inside above and imaged immediately. The mean fluorescence intensity of the tumors was calculated using *Living Image* software.

Tissue Analysis. Twenty-four hours post-injection of siNEG AF546 in different formulations, the mice were killed and tumors samples were collected. Samples were stored at -80 $^{\circ}$ C prior to frozen sectioning. Frozen tumors were embedded into OCT and plunged into a liquid-nitrogen bath for at least 30 s. Samples were retrieved from the bath then sectioned using the cryostat at -18 $^{\circ}$ C into 10- μ m-thick sections. The sections were mounted on a superfrost slide and left to dry at room temperature for 15–30 min. For tumor visualization, the sections were fixed for 3 min in cold acetone at -20 $^{\circ}$ C, rinsed with PBS for 15 min at room temperature, and mounted with Vectashield as a mounting medium. Nuclei were Nucleus counterstained with DAPI. The slices were visualized under 40 \times lens using CLSM (LSM 710, Zeiss UK). DAPI and AlexaFluor546 were excited at 4% of 365 and 5% of 514 laser power, respectively.

■ ASSOCIATED CONTENT

■ Supporting Information

SI Figure 1: Chemical structures and TEM images of positively charged *f*-MWNT (MWNT-NH₃⁺). SI Figure 2: Histological examination of the major organs in tumor-bearing mice. SI Figure 3: Quantification of the fluorescence signals detected in the tumor region in xenograft-bearing mice after intratumoral administration. The Supporting Information is available free of charge on the ACS Publications website at DOI: 10.1021/acs.bioconjchem.5b00249.

■ AUTHOR INFORMATION

Corresponding Authors

*E-mail: k.kostarelos@ucl.ac.uk, kostas.kostarelos@manchester.ac.uk.

*E-mail: khuloud.al-jamal@kcl.ac.uk.

Present Address

#Khuloud T. Al-Jamal, Institute of Pharmaceutical Science, Franklin-Wilkins Building, King's College London, London SE1 9NH, UK

Notes

The authors declare no competing financial interest.

■ ACKNOWLEDGMENTS

The work has been supported partially by the School of Pharmacy, University of London, the University of Trieste, Italian Ministry of Education MIUR (cofin Prot. 2008SM27SS and firb prot. RBAP11ETKA) and Regione Friuli Venezia Giulia, the Centre National de la Recherche Scientifique (CNRS) and the European Union FP7 ANTICARB (FP7-HEALTH-2007-2.4.1-7) research programme. M.P. acknowledges financial support from ERC Advanced Grant Carbonanobridge (ERC-2008-AdG-227135).

■ REFERENCES

- (1) Iannazzo, D., Piperno, A., Pistone, A., Grassi, G., and Galvagno, S. (2013) Recent advances in carbon nanotubes as delivery systems for anticancer drugs. *Curr. Med. Chem.* 20, 1333–54.
- (2) Koff, J. L., Ramachandiran, S., and Bernal-Mizrachi, L. (2015) A Time to Kill: Targeting Apoptosis in Cancer. *Int. J. Mol. Sci.* 16, 2942–2955.
- (3) Bremer, E., van Dam, G., Kroesen, B. J., de Leij, L., and Helfrich, W. (2006) Targeted induction of apoptosis for cancer therapy: current progress and prospects. *Trends Mol. Med.* 12, 382–93.
- (4) Zhang, H., Shi, X., Paddon, H., Hampong, M., Dai, W., and Pelech, S. (2004) B23/nucleophosmin serine 4 phosphorylation mediates mitotic functions of polo-like kinase 1. *J. Biol. Chem.* 279, 35726–34.
- (5) Cheng, L., Wang, C., and Jing, J. (2014) Polo-like kinase 1 as a potential therapeutic target for osteosarcoma. *Curr. Pharm. Des.* 21, 1347–1350.
- (6) Golsteyn, R. M., Schultz, S. J., Bartek, J., Ziemiecki, A., Ried, T., and Nigg, E. A. (1994) Cell cycle analysis and chromosomal localization of human Plk1, a putative homologue of the mitotic kinases *Drosophila* polo and *Saccharomyces cerevisiae* Cdc5. *J. Cell Sci.* 107 (Pt 6), 1509–17.
- (7) Holtrich, U., Wolf, G., Brauning, A., Karn, T., Bohme, B., Rubsam, H., and Strebhardt, K. (1994) Induction and down-regulation of PLK, a human serine/threonine kinase expressed in proliferating cells and tumors. *Proc. Natl. Acad. Sci. U. S. A.* 91, 1736–40.
- (8) Garland, L. L., Taylor, C., Pilkington, D. L., Cohen, J. L., and Von Hoff, D. D. (2006) A phase I pharmacokinetic study of HMN-214, a novel oral stilbene derivative with polo-like kinase-1-interacting

properties, in patients with advanced solid tumors. *Clin. Cancer Res.* 12, 5182–9.

(9) Ahmad, N. (2004) Polo-like kinase (Plk) 1: a novel target for the treatment of prostate cancer. *FASEB J.* 18, 5–7.

(10) Reagan-Shaw, S., and Ahmad, N. (2005) Polo-like kinase (Plk) 1 as a target for prostate cancer management. *IUBMB Life* 57, 677–682.

(11) Spankuch-Schmitt, B., Bereiter-Hahn, J., Kaufmann, M., and Strebhardt, K. (2002) Effect of RNA silencing of polo-like kinase-1 (PLK1) on apoptosis and spindle formation in human cancer cells. *J. Natl. Cancer Inst.* 94, 1863–77.

(12) Spankuch-Schmitt, B., Wolf, G., Solbach, C., Loibl, S., Knecht, R., Stegmüller, M., von Minckwitz, G., Kaufmann, M., and Strebhardt, K. (2002) Downregulation of human polo-like kinase activity by antisense oligonucleotides induces growth inhibition in cancer cells. *Oncogene* 21, 3162–71.

(13) Hu, K., Law, J. H., Fotovati, A., and Dunn, S. E. (2012) Small interfering RNA library screen identified polo-like kinase-1 (PLK1) as a potential therapeutic target for breast cancer that uniquely eliminates tumor-initiating cells. *Breast Cancer Res.* 14, R22.

(14) Maire, V., Nemat, F., Richardson, M., Vincent-Salomon, A., Tesson, B., Rigault, G., Gravier, E., Marty-Prouvost, B., De Koning, L., Lang, G., et al. (2013) Polo-like kinase 1: a potential therapeutic option in combination with conventional chemotherapy for the management of patients with triple-negative breast cancer. *Cancer Res.* 73, 813–23.

(15) Al-Jamal, K. T., Gherardini, L., Bardi, G., Nunes, A., Guo, C., Bussy, C., Herrero, M. A., Bianco, A., Prato, M., Kostarelos, K., et al. (2011) Functional motor recovery from brain ischemic insult by carbon nanotube-mediated siRNA silencing. *Proc. Natl. Acad. Sci. U.S.A.* 108, 10952–7.

(16) Kostarelos, K., Bianco, A., and Prato, M. (2009) Promises, facts and challenges for carbon nanotubes in imaging and therapeutics. *Nat. Nanotechnol.* 4, 627–33.

(17) Kam, N. W., Liu, Z., and Dai, H. (2005) Functionalization of carbon nanotubes via cleavable disulfide bonds for efficient intracellular delivery of siRNA and potent gene silencing. *J. Am. Chem. Soc.* 127, 12492–3.

(18) Zhang, Z., Yang, X., Zhang, Y., Zeng, B., Wang, S., Zhu, T., Roden, R. B., Chen, Y., and Yang, R. (2006) Delivery of telomerase reverse transcriptase small interfering RNA in complex with positively charged single-walled carbon nanotubes suppresses tumor growth. *Clin. Cancer Res.* 12, 4933–9.

(19) Wang, X., Ren, J., and Qu, X. (2008) Targeted RNA interference of cyclin A2 mediated by functionalized single-walled carbon nanotubes induces proliferation arrest and apoptosis in chronic myelogenous leukemia K562 cells. *ChemMedChem* 3, 940–5.

(20) Chen, H., Ma, X., Li, Z., Shi, Q., Zheng, W., Liu, Y., and Wang, P. (2012) Functionalization of single-walled carbon nanotubes enables efficient intracellular delivery of siRNA targeting MDM2 to inhibit breast cancer cells growth. *Biomed. Pharmacotherapy* 66, 334–8.

(21) Wang, L., Shi, J., Zhang, H., Li, H., Gao, Y., Wang, Z., Wang, H., Li, L., Zhang, C., Chen, C., et al. (2013) Synergistic anticancer effect of RNAi and photothermal therapy mediated by functionalized single-walled carbon nanotubes. *Biomaterials* 34, 262–74.

(22) Podesta, J. E., Al-Jamal, K. T., Herrero, M. A., Tian, B., Ali-Boucetta, H., Hegde, V., Bianco, A., Prato, M., and Kostarelos, K. (2009) Antitumor activity and prolonged survival by carbon-nanotube-mediated therapeutic siRNA silencing in a human lung xenograft model. *Small* 5, 1176–85.

(23) Al-Jamal, K. T., Toma, F. M., Yilmazer, A., Ali-Boucetta, H., Nunes, A., Herrero, M. A., Tian, B., Eddaoudi, A., Al-Jamal, W. T., Bianco, A., et al. (2010) Enhanced cellular internalization and gene silencing with a series of cationic dendron-multiwalled carbon nanotube:siRNA complexes. *FASEB J.* 24, 4354–65.

(24) Battigelli, A., Wang, J. T., Russier, J., Da Ros, T., Kostarelos, K., Al-Jamal, K. T., Prato, M., and Bianco, A. (2013) Ammonium and guanidinium dendron-carbon nanotubes by amidation and click chemistry and their use for siRNA delivery. *Small* 9, 3610–9.

(25) Bartholomeusz, G., Cherukuri, P., Kingston, J., Cognet, L., Lemos, R., Leeuw, T. K., Gumbiner-Russo, L., Weisman, R. B., and Powis, G. (2009) In vivo therapeutic silencing of hypoxia-inducible factor 1 alpha (HIF-1alpha) using single-walled carbon nanotubes noncovalently coated with siRNA. *Nano Res.* 2, 279–291.

(26) Al-Jamal, K. T., Toma, F. M., Yilmazer, A., Ali-Boucetta, H., Nunes, A., Herrero, M. A., Tian, B., Eddaoui, A., Al-Jamal, W. T., Bianco, A., et al. (2010) Enhanced cellular internalization and gene silencing with a series of cationic dendron-multiwalled carbon nanotube:siRNA complexes. *FASEB J.* 24, 4354–4365.

(27) Herrero, M. A., Toma, F. M., Al-Jamal, K. T., Kostarelos, K., Bianco, A., Da Ros, T., Bano, F., Casalis, L., Scoles, G., and Prato, M. (2009) Synthesis and characterization of a carbon nanotube-dendron series for efficient siRNA delivery. *J. Am. Chem. Soc.* 131, 9843–8.

(28) Zimmermann, T. S., Lee, A. C., Akinc, A., Bramlage, B., Bumcrot, D., Fedoruk, M. N., Harborth, J., Heyes, J. A., Jeffs, L. B., John, M., et al. (2006) RNAi-mediated gene silencing in non-human primates. *Nature* 441, 111–4.

(29) Bao, A. D., Phillips, W. T., Goins, B., Zheng, X. P., Sabour, S., Natarajan, M., Woolley, F. R., Zavaleta, C., and Otto, R. A. (2006) Potential use of drug carried-liposomes for cancer therapy via direct intratumoral injection. *Int. J. Pharm.* 316, 162–169.

(30) aalLanner, J. T., Bruton, J. D., Assefaw-Redda, Y., Andronache, Z., Zhang, S. J., Severa, D., Zhang, Z. B., Melzer, W., Zhang, S. L., Katz, A., et al. (2009) Knockdown of TRPC3 with siRNA coupled to carbon nanotubes results in decreased insulin-mediated glucose uptake in adult skeletal muscle cells. *FASEB J.* 23, 1728–38.

(31) Cai, D., Mataraza, J. M., Qin, Z. H., Huang, Z. P., Huang, J. Y., Chiles, T. C., Carnahan, D., Kempa, K., and Ren, Z. F. (2005) Highly efficient molecular delivery into mammalian cells using carbon nanotube spearing. *Nat. Methods* 2, 449–454.

(32) Liu, Z., Winters, M., Holodniy, M., and Dai, H. (2007) siRNA delivery into human T cells and primary cells with carbon-nanotube transporters. *Angew. Chem., Int. Ed.* 46, 2023–7.

(33) Krajcik, R., Jung, A., Hirsch, A., Neuhuber, W., and Zolk, O. (2008) Functionalization of carbon nanotubes enables non-covalent binding and intracellular delivery of small interfering RNA for efficient knock-down of genes. *Biochem. Biophys. Res. Commun.* 369, 595–602.

(34) Ladeira, M. S., Andrade, V. A., Gomes, E. R., Aguiar, C. J., Moraes, E. R., Soares, J. S., Silva, E. E., Lacerda, R. G., Ladeira, L. O., Jorio, A., et al. (2010) Highly efficient siRNA delivery system into human and murine cells using single-wall carbon nanotubes. *Nanotechnology* 21, 385101.

(35) Kurizaki, T., Okazaki, S., Sanderson, S. D., Colcher, D., Enke, C. A., Tempero, M. A., and Baranowska-Kortylewicz, J. (2002) Potentiation of radioimmunotherapy with response-selective peptide agonist of human CSa. *J. Nucl. Med.* 43, 957–67.

(36) Wu, J., and Houghton, P. J. (2009) Assessing cytotoxic treatment effects in preclinical tumor xenograft models. *J. Biopharm. Stat.* 19, 755–62.